Available online at www.sciencedirect.com
ScienceDirect
International Journal of Heat and Mass Transfer 51 (2008) 2282–2298
International Journal of HEAT and MASS TRANSFER
www.elsevier.com/locate/ijhmt

Transport of a train of short-pulse radiation of step temporal profile through a 2-D participating medium

R. Muthukumaran, Subhash C. Mishra *

Department of Mechanical Engineering, Indian Institute of Technology, Guwahati 781 039, India

Received 15 May 2007; received in revised form 6 August 2007
Available online 23 October 2007

Abstract

This article deals with the transport of a train of short-pulse radiation through a 2-D rectangular participating medium. The diffuse as well as collimated incident short-pulse radiations are considered. Temporal profile at the boundary of incidence is a step function. The pulse train consists of 1–4 pulses. The homogeneous participating medium is absorbing, and scattering. Both diffuse and collimated pulse trains with pulse width of the order of a nano-second are considered. Transmittance and reflectance signals are analyzed for the effects of the extinction coefficient and the scattering albedo. Heat flux distributions inside the medium are also studied. The finite volume method is used to solve the problem.

1. Introduction

In recent times, developments of many new technologies can be attributed micro- and nano-scale engineering. Some applications of such technologies are micro-fabrication, non-destructive testing, remote sensing and bio-medical diagnostics [1,2]. In these, the spatial dimensions range from O(10^{-6} m) to O(10^{-9} m) and the temporal dimensions range from O(1 s) to O(10^{-18} s). The developments of these technologies require a proper understanding of the spatial and temporal distributions of various quantities.

Diagnosis using a very short-pulse thermal radiations is one of non-invasive techniques being explored these days to characterize optically participating tissues and turbid media [2–36]. As far as imaging of the tumors in a living tissue is concerned, short-pulse thermal radiation imaging is believed to have advantages of economic viability, compact set up and no side effect over established techniques such as X-ray computed tomography, ultrasound and MRI [22]. Apart from these, short-pulse thermal radiation finds applications in laser tissue welding [3–5], laser tissue soldering [5,6,22], laser tissue ablation [6,22], photodynamic therapy [22] and remote sensing [10,13,14], to name a few.

A good amount of literature has been devoted to the study of interaction of a short-pulse radiation with an optically participating medium. Both homogeneous [14–23,26,27] and inhomogeneous [24] media have been considered [4,5,8–34]. Although most of the studies have focused on a simple 1-D planar geometry [14,18,22,26–29,32–34], some studies have also been reported for 2-D [17,20,21] and 3-D Cartesian geometries [24,30]. In these studies, various numerical radiative transfer methods such as the spherical harmonics method (P_N approximation), the discrete ordinates method (DOM), the discrete transfer method (DTM), the Monte Carlo method (MCM), the radiation element method and the finite volume method (FVM) have been employed, and mostly the analyses were carried out for a single-pulse radiation.

Recently Muthukumaran and Mishra [32–34] have studied the interaction of a short-pulse radiation train with 1-D homogeneous and inhomogeneous participating media. They analyzed the problems with diffuse as well as collimated (laser) radiations and considered both step as well

* Corresponding author. Tel.: +91 361 2582660; fax: +91 361 2690762.
E-mail address: scm_iitg@yahoo.com (S.C. Mishra).

0017-9310/$ - see front matter © 2007 Elsevier Ltd. All rights reserved.
doi:10.1016/j.ijheatmasstransfer.2007.08.032

Nomenclature

a	anisotropy factor
c	speed of light
G	incident radiation
H	heaviside function
I	intensity
I_b	blackbody intensity, $\frac{\sigma T^4}{\pi}$
$\hat{i}, \hat{j}, \hat{k}$	unit vectors in x, y-, z-directions, respectively
M	number of discrete directions
N	total number of pulses in a pulse train
p	scattering phase function
$\hat{n}$	outward normal
q	heat flux
S	source term
s	geometric distance in the direction of the intensity
T	temperature
T_p	time period of a pulse train
t	time
t_p	pulse-width
X, Y	physical dimensions of the medium in x- and y-directions
x, y	x- and y-coordinate directions

Greek symbols

β	extinction coefficient
δ	Dirac-delta function
κ_a	absorption coefficient
ε	emissivity
θ	polar angle
σ	Stefan–Boltzmann constant $= 5.67 \times 10^{-8}$ W/m^2 K^4
σ_s	scattering coefficient
Ω	direction (θ, ϕ)
$\Delta\Omega$	solid angle, $\sin\theta \, d\theta \, d\phi$
ω	scattering albedo $\left(=\frac{\sigma_s}{\beta}\right)$
ϕ	azimuthal angle

Subscripts

c	collimated
d	diffuse
E, W, N, S	east, west, north, south
P	cell center
r	reflectance
t	transmittance
w	wall/boundary

Superscripts

m	index for the discrete direction
*	dimensionless quantity

as Gaussian temporal profiles of the incident pulses. Unlike, a single-pulse, the pulse train was found to provide additional information about the medium.

A 2-D geometry represents more realistic situation, but on the other hand, it brings additional mathematical complexities. Analyses of a short-pulse radiation in a 2-D rectangular geometry have been reported in [17,20,21]. In these studies, the MCM, P-1 approximation and the DOM have been used. These analyses were reported for a single-pulse radiation.

The FVM, though an offshoot of the DOM, is computationally more expensive due to the integration of the direction cosine over the elemental solid angle. This integration minimizes the ray effect and eliminates false scattering which are the two main drawbacks of the DOM. Further because of integration over control volumes and solid angles, unlike other methods, the FVM is fully conservative and is thus well suited for a large class of problems dealing with radiative transfer including transient radiative transfer.

As far as the 2-D rectangular geometries are concerned, so far no work has been focused on the study of the effect of multiple pulses on transmittance and reflectance signals. The present work is therefore aimed at the analysis of interaction of a short-pulse laser train in a 2-D rectangular participating medium. To see the effects of different number of pulses, the pulse train is assumed to be consisting of 1–4 pulses. Further to study the nature of the originating signals, both diffuse as well as collimated radiations are considered. The temporal profiles of these pulses are considered to be a step function. The FVM is used to analyze the problem.

2. Formulation

We consider the south boundary of the 2-D rectangular (Fig. 1a) absorbing, emitting and scattering participating medium subjected to a pulse radiation. As shown in Figs. 2b and c, the pulse radiation at the south boundary can either be diffuse or collimated. The temporal profile of the pulse radiation is a step function (Fig. 1d). The pulse train consists of 1–4 pulses. The pulse-width t_p of the incident radiation is of the order of 10^{-9} s. The half-time period of the pulse train is taken the same as the pulse width t_p (Fig. 1d).

Since the radiation source at the south boundary is available for a very short time, $O(10^{-9}\text{ s})$, although it travels with the speed of light ($c = 3 \times 10^8$ m/s), its propagation in the medium is a transient phenomenon. The radiation signals at any point in the medium including the boundaries are thus short-lived and their magnitudes

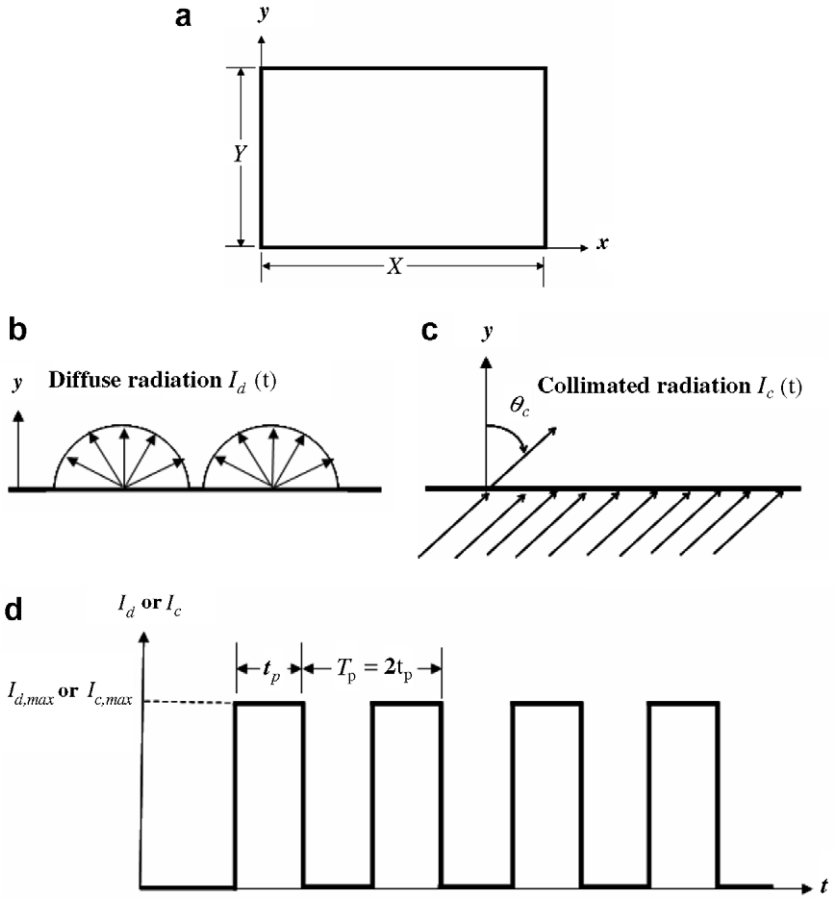

Fig. 1. (a) 2-D Geometry and the coordinate system under consideration; (b) south boundary subjected to a short-pulse diffuse radiation, (c) south boundary subjected to a short-pulse collimated radiation; (d) temporal profile of a 4-pulse train.

are strong functions of time. In this situation, the radiative transfer equation (RTE) is given by

$$\left(\frac{1}{c}\right)\frac{\partial I}{\partial t}+\frac{\partial I}{\partial s}=-\beta I+\kappa_{\mathrm{a}}I_{\mathrm{b}}+\frac{\sigma_{\mathrm{s}}}{4\pi}\int_{4\pi}Ip(\Omega,\Omega')\,\mathrm{d}\Omega' \tag{1}$$

where s is the geometric distance in the direction $\hat{s}=(\sin\theta\cos\phi)\hat{i}+(\sin\theta\sin\phi)\hat{j}+\cos\theta\hat{k}$, κ_{a} is the absorption coefficient, β is the extinction coefficient, σ_{s} is the scattering coefficient and p is the scattering phase function.

In the present work we have considered the south boundary of the 2-D medium subjected to either diffuse or collimated radiation. In the following pages, we provide a formulation for the latter case which is more general. The change in the formulation for the diffuse radiation is highlighted wherever it is necessary.

The transport of the collimated radiation in the medium and its decay results in diffuse radiation. Thus within the medium, the intensity I is composed of two components, *viz.*, the collimated intensity I_{c} and the diffuse intensity I_{d}.

$$I=I_{\mathrm{c}}+I_{\mathrm{d}} \tag{2}$$

The change of the collimated intensity I_{c} in the medium is governed by

$$\left(\frac{1}{c}\right)\frac{\partial I_{\mathrm{c}}}{\partial t}+\frac{\partial I_{\mathrm{c}}}{\partial s}=-\beta I_{\mathrm{c}} \tag{3}$$

From Eqs. (1)–(3), we get

$$\left(\frac{1}{c}\right)\frac{\partial I_{\mathrm{d}}}{\partial t}+\frac{\partial I_{\mathrm{d}}}{\partial s}=-\beta I_{\mathrm{d}}+S_{\mathrm{c}}+S_{\mathrm{d}}=-\beta I_{\mathrm{d}}+S_{\mathrm{t}} \tag{4}$$

where S_{c} and S_{d} are the source terms resulting from the collimated and the diffuse components of radiation, respectively. In Eq. (4), $S_{\mathrm{t}}=S_{\mathrm{c}}+S_{\mathrm{d}}$ is the total source term. The source term S_{c} resulting from the collimated radiation I_{c}, in terms of the incident radiation G_{c} and heat flux q_{c}, for a linear anisotropic phase function $p(\Omega,\Omega')=1+a\cos\theta\cos\theta'$ is given by

$$\begin{aligned}S_{\mathrm{c}}(t)&=\frac{\sigma_{\mathrm{s}}}{4\pi}\int_{\Omega'=0}^{4\pi}I_{\mathrm{c}}(\Omega,t)p(\Omega,\Omega')\,\mathrm{d}\Omega'\\&=\frac{\sigma_{\mathrm{s}}}{4\pi}[G_{\mathrm{c}}(t)+a\cos\theta q_{\mathrm{c}}(t)]\end{aligned} \tag{5}$$

In Eq. (5), G_{c} and q_{c} are given by

$$G_{\mathrm{c}}(t)=I_{\mathrm{c}}(\theta,\phi,t) \tag{6}$$

$$q_{\mathrm{c}}(t)=I_{\mathrm{c}}(\theta,\phi,t)\cos\theta \tag{7}$$

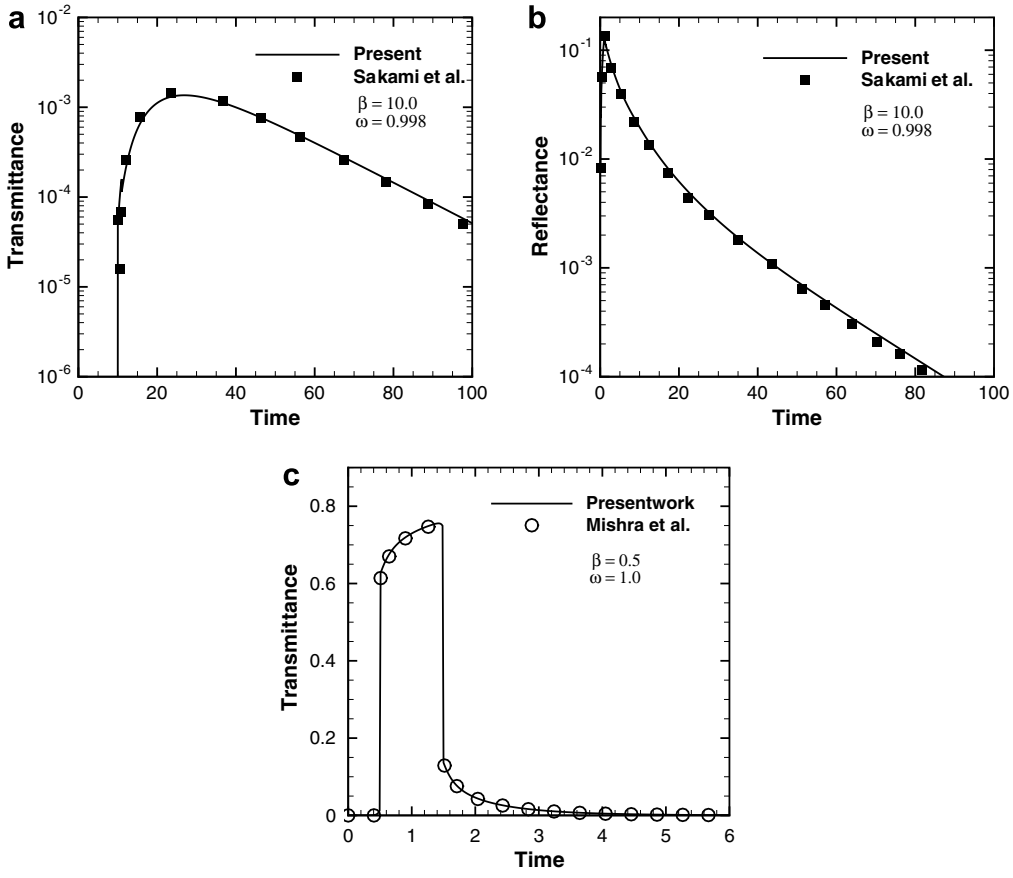

Fig. 2. Comparison of (a) transmittance $q_t^*(0.5, 1.0, t^*)$ for $\frac{X}{Y} = 1$, (b) reflectance $q_r^*(0.5, 0.0, t^*)$ for $\frac{X}{Y} = 1$ and (c) transmittance $q_t^*(0.5, 1.0, t^*)$ for $\frac{X}{Y} = 100$ signals in a 2-D medium.

where

$$\begin{aligned} I_c(\theta,\phi,t) &= I_{c,\max}(\theta,\phi,t)\exp(-\beta s_c)[H\{\beta(ct-(N-1)T_p-s_c)\} \\ &\quad - H\{\beta(ct-(N-1)T_p-s_c)-\beta ct_p\}] \\ &\quad \times \delta(\theta-\theta_c)\times\delta(\phi-\phi_c) \end{aligned} \tag{8}$$

where in Eq. (8), $I_{c,\max}$ is the collimated intensity at the south boundary, s_c is the geometric distance in the direction (θ_c, ϕ_c) of the collimated radiation, δ is the Dirac-delta function and H is the Heaviside function.

If $t^* = \beta ct$ and $t_p^* = \beta ct_p$ are the dimensionless times, Eq. (8) can be written as

$$\begin{aligned} I_c(\theta,\phi,t^*) &= I_{c,\max}(\theta,\phi,t^*)\exp(-\beta s_c)\times[H\{t^*-(N-1)T_p^*-\beta s_c\} \\ &\quad - H\{t^*-\beta s_c-(N-1)T_p^*-t_p^*\}] \\ &\quad \times\delta(\theta-\theta_c)\times\delta(\phi-\phi_c) \end{aligned} \tag{9}$$

where in Eq. (9), N is the number of pulses and $T_p^* = \beta cT_p$ is the dimensionless time period of the pulse train.

In Eq. (4), for the linear anisotropic phase function $p(\Omega, \Omega') = 1 + a\cos\theta\cos\theta'$, the source term S_d in terms of incident radiation G_d and heat flux q_d resulting from the diffuse radiation I_d is given by

$$S_d(t^*) = \kappa_a I_b(t^*) + \frac{\sigma_s}{4\pi}[G_d(t^*) + a\cos\theta q_d(t^*)] \tag{10}$$

In Eq. (10), G_d and q_d are given by and numerically computed from [35]

$$G_d(t^*) \approx \sum_{l=1}^{M_\phi}\sum_{k=1}^{M_\theta} I_d(\theta_k^m,\phi_l^m,t^*)2\sin\theta_k^m\sin\left(\frac{\Delta\theta_k^m}{2}\right)\Delta\phi_l^m \tag{11}$$

$$q_d(t^*) \approx \sum_{l=1}^{M_\phi}\sum_{k=1}^{M_\theta} I_d(\theta_k,\phi_l,t^*)\sin\theta_k^m\cos\theta_k^m\sin\Delta\theta_k^m\Delta\phi_l^m \tag{12}$$

where M_θ and M_ϕ are the number of discrete points considered over the complete span of the polar angle ($0 \leqslant \theta \leqslant \pi$)and azimuthal angle ($0 \leqslant \phi \leqslant 2\pi$), respectively. Therefore, $M_\theta \times M_\phi$ constitute the number of discrete directions in which intensities are considered at any point.

For a boundary having temperature T_w and emissivity ε_w, the boundary intensity $I_d(r_w, t^*)$ is given by and computed from

$$\begin{aligned} I_d(r_w,t^*) \approx \frac{\varepsilon_w\sigma T_w^4}{\pi} + \left(\frac{1-\varepsilon_w}{\pi}\right)\sum_{l=1}^{M_\phi}\sum_{k=1}^{M_\theta/2}[I_{d,w}(\theta_k^m,\phi_l^m,t^*) \\ + I_{c,w}(\theta_k^m,\phi_l^m,t^*)]\sin\theta_k^m\cos\theta_k^m\sin\Delta\theta_k^m\Delta\phi_l^m \end{aligned} \tag{13}$$

where in Eq. (13), the first and the second terms represent emitted and reflected components of the boundary intensity, respectively.

In terms of non-dimensional time t^*, the RTE given in Eq. (4) for a discrete direction (θ_k^m, ϕ_l^m) with index m is now written as

$$\beta\frac{\partial I_{\mathrm{d}}^m}{\partial t^*}+\frac{\partial I_{\mathrm{d}}^m}{\partial s^m}+\beta I_{\mathrm{d}}^m=S_{\mathrm{t}}^m \tag{14}$$

Using backward differencing scheme in time, Eq. (14) becomes

$$\beta\frac{I_{\mathrm{d}}^m(t^*)-I_{\mathrm{d}}^m(t^*-\Delta t^*)}{\Delta t^*}+\frac{\partial I_{\mathrm{d}}^m(t^*)}{\partial s^m}+\beta I_{\mathrm{d}}^m(t^*)=S_{\mathrm{t}}^m(t^*) \tag{15}$$

Eq. (15) is written in simplified form as

$$B\frac{\partial I_{\mathrm{d}}^m(t^*)}{\partial s^m}+\beta I_{\mathrm{d}}^m(t^*)=BS_{\mathrm{t}}^m(t^*)+CI_{\mathrm{d}}^m(t^*-\Delta t^*) \tag{16}$$

where $B=\frac{\Delta t^*}{(1+\Delta t^*)}$ and $C=\frac{\beta}{1+\Delta t^*}$.

Below we briefly present formulation and methodology to solve Eq. (16) using the FVM. Details of this method specially for transient radiative transfer can be found in Mishra et al. [25] and for a steady-state radiative transport problems, the same can be found in Chai and Patankar [36] and Mishra and Roy [35].

Resolving Eq. (16) in x- and y- Cartesian coordinate directions and integrating over the elemental solid angle $\Delta\Omega^m$, we get

$$B\left[\frac{\partial I_{\mathrm{d}}^m(t^*)}{\partial x}D_x^m+\frac{\partial I_{\mathrm{d}}^m(t^*)}{\partial y}D_y^m\right]+\beta I_{\mathrm{d}}^m(t^*) =[BS_{\mathrm{t}}^m(t^*)+CI_{\mathrm{d}}^m(t^*-\Delta t^*)]\Delta\Omega^m \tag{17}$$

When the outward normal $\hat{n}$ is pointing towards one of the positive coordinate directions, D_x^m and D_y^m are given by Mishra and Roy [35]

$$D_x^m=\cos\phi^m\sin\left(\frac{\Delta\phi^m}{2}\right)[\Delta\theta^m-\cos 2\theta^m\sin(\Delta\theta^m)] \tag{18}$$

$$D_y^m=\sin\phi^m\sin\left(\frac{\Delta\phi^m}{2}\right)[\Delta\theta^m-\cos 2\theta^m\sin(\Delta\theta^m)] \tag{19}$$

For $\hat{n}$ pointing towards the negative coordinate directions, signs of D_x^m and D_y^m are negative. In Eq. (17), $\Delta\,\Omega^m$ is given by

$$\Delta\Omega^m=2\sin\theta^m\sin\left(\frac{\Delta\theta^m}{2}\right)\Delta\phi^m \tag{20}$$

Integrating Eq. (17) over the 2-D control volume ($\mathrm{d}V=\mathrm{d}x\times y\times 1$), we get

$$[I_{\mathrm{d,\,E}}^m(t^*)-I_{\mathrm{d,\,W}}^m(t^*)]A_xD_x^m+[I_{\mathrm{d,\,N}}^m(t^*)-I_{\mathrm{d,\,S}}^m(t^*)]A_yD_y^m =\left[-\frac{\beta}{B}I_{\mathrm{d,\,P}}^m(t^*)+S_{\mathrm{t,\,P}}^m+\frac{C}{B}I_{\mathrm{d,\,P}}^m(t^*-\Delta t^*)\right]\mathrm{d}V\Delta\Omega^m \tag{21}$$

where A_x and A_y are the areas of the x- and y-faces of he 2-D control volume, respectively. In Eq. (21), I with suffixes E, W, N and S designate east, west, north and south control surface average intensities, respectively. On the right-hand side of Eq. (14), I_{P}^m and S_{P}^m are the volume averaged intensity and source term at the cell centre 'P', respectively.

To reduce the number of unknowns in Eq. (21), in a given direction, in a control volume, a relationship is sought among surface average intensities and the volume averaged intensity. The common practice in the FVM is to use a diamond differencing scheme. For 2-D control volumes considered in the present problem, thus we have:

$$I_{\mathrm{d,\,P}}^m=\frac{I_{\mathrm{d,\,N}}^m+I_{\mathrm{d,\,S}}^m}{2}=\frac{I_{\mathrm{d,\,E}}^m+I_{\mathrm{d,\,W}}^m}{2} \tag{22}$$

From Eqs. (21) and (22), a general expression of $I_{\mathrm{d},P}^m(t^*)$in terms of known surface average intensities and source terms is written as [35]

$$I_{\mathrm{d,\,P}}^m(t^*)=\frac{\left[|D_x^m|A_xI_{\mathrm{d},x_i}^m(t^*)+\left|D_y^m\right|A_yI_{\mathrm{d},y_i}^m(t^*)+\left(\frac{V\Delta\Omega^m}{2}\right)S_{\mathrm{t,\,P}}^m(t^*)+\left(\frac{CV\Delta\Omega^m}{2B}\right)I_{\mathrm{d,\,P}}^m(t^*-\Delta t^*)\right]}{|D_x^m|A_x+|D_y^m|A_y+\left(\frac{\beta V\Delta\Omega^m}{2B}\right)} \tag{23}$$

where in Eq. (23), x_i and y_i suffixes over I_{d}^m are for the intensities entering the control volume through x- and y-faces, respectively.

2.1. Solution procedure

Temporal signals at the boundary of incidence and the opposite boundary are termed as reflectance $q_{\mathrm{r}}^*\left(\frac{x}{X},0,t^*\right)$ and transmittance $q_{\mathrm{t}}^*\left(\frac{x}{X},1,t^*\right)$, respectively. These are the two important signals normally analyzed and they are the radiative fluxes at the respective boundaries because of the radiative contributions from the medium. Further, heat flux $q^*\left(\frac{x}{X},\frac{y}{Y},t^*\right)$ distributions inside the medium also provide some useful information. For any dimensionless timet^*, in non-dimensional form, they are defined as

$$\text{Reflectance:}\quad q_{\mathrm{r}}^*\left(\frac{x}{X},0,t^*\right)=\frac{q_{\mathrm{d}}\left(\frac{x}{X},0,t^*\right)}{q_{in}\left(\frac{x}{X},0,t^*\right)} \tag{24}$$

$$\text{Transmittance:}\quad q_{\mathrm{t}}^*\left(\frac{x}{X},1,t^*\right)=\frac{q_{\mathrm{c}}\left(\frac{x}{X},1,t^*\right)+q_{\mathrm{d}}\left(\frac{x}{X},1,t^*\right)}{q_{in}\left(\frac{x}{X},0,t^*\right)} \tag{25}$$

$$\text{Heat flux:}\quad q^*\left(\frac{x}{X},\frac{y}{Y},t^*\right)=\frac{q_{\mathrm{c}}\left(\frac{x}{X},\frac{y}{Y},t^*\right)+q_{\mathrm{d}}\left(\frac{x}{X},\frac{y}{Y},t^*\right)}{q_{in}\left(\frac{x}{X},0,t^*\right)} \tag{26}$$

where $q_{in}\left(\frac{x}{X},0,t^*\right)$ is the flux input to the medium through the boundary of incidence (south boundary).

The time marching and ray tracing procedures have been adopted from Mishra et al. [25] and Mishra and Roy [35] and the same are not repeated here.

3. Results and discussion

For grid independent, 50×50 equal size control volumes were used and a maximum of 120 directions covering the 4π solid angle were found enough for the ray-independent solutions. 1000 divisions of the total time t^* domain were found sufficient for marching in the time dimension. At every time step, the iteration was set to $|S^m_{\text{t, old, P}} - S^m_{\text{t,new,P}}| \leqslant 1.0 \times 10^{-7}$.

The code written in Turbo C++ was executed on a Xeon 300 dual processor 800 MHz computer. To study the computational time, the CPU times were recorded for all the cases. The CPU times for optically thin ($\beta = 1.0$) to thick ($\beta = 10.0$) cases ranged from 55 s to 280 s, respectively.

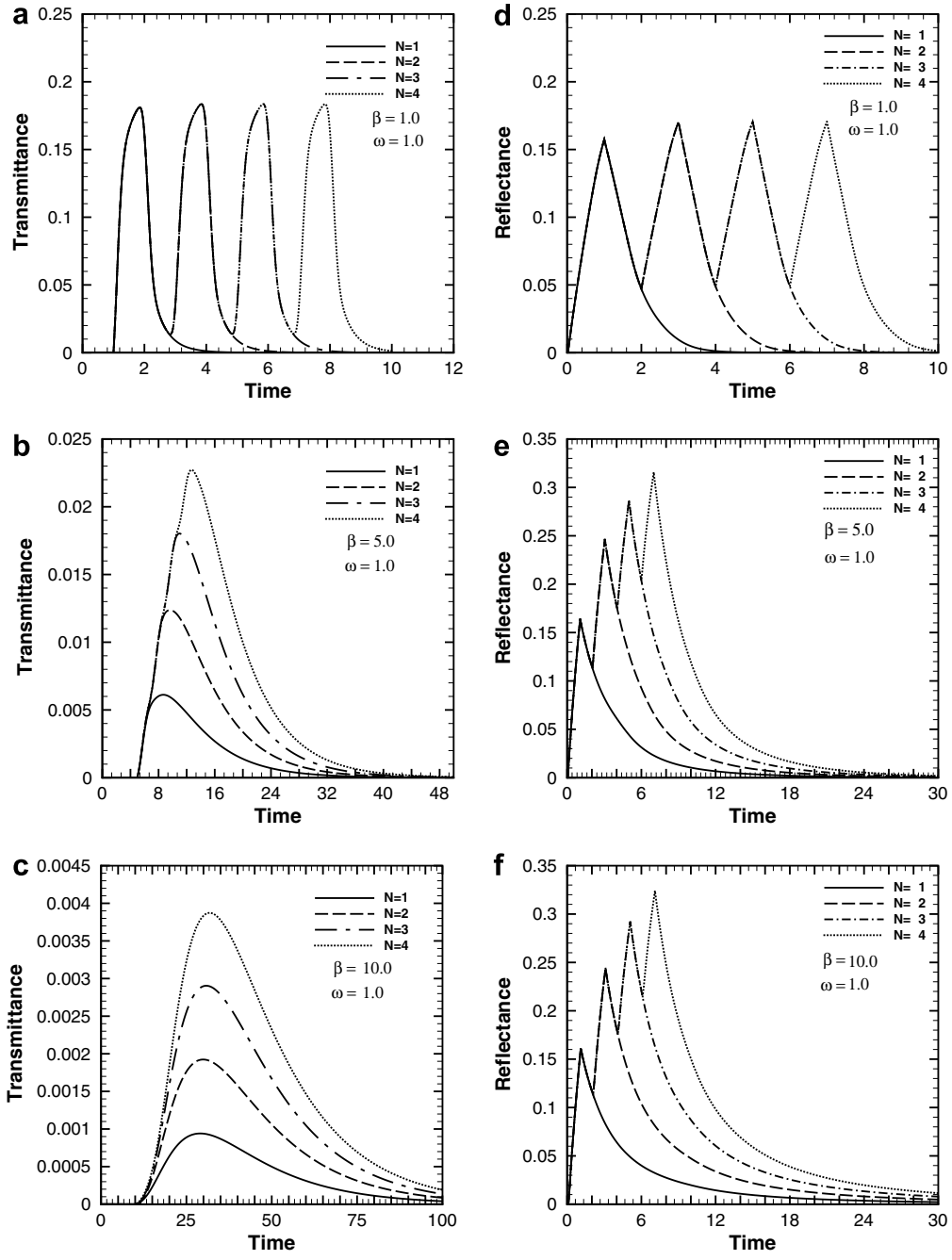

Fig. 3. Transmittance $q^*_t(0.5, 1.0, t^*)$ signals and reflectance $q^*_r(0.5, 0.0, t^*)$ signals for 1–4 pulses for three different values of extinction coefficient β. The south boundary subjected to diffuse radiation.

3.1. Validation of results

First we validate the results of the present work for a single-pulse with those available in the literature. For a square medium $\left(\frac{X}{Y}=1\right)$ subjected to a single laser (collimated radiation) pulse, Figs. 2a and b show comparison of the present results with those of Sakami et al. [21] obtained using the DOM with high order upwind piecewise parabolic interpolation scheme. In Fig. 2c and d, transmittance results of the present 2-D code have been compared with those from Mishra et al. [25] and Muthukumaran and Mishra [32] for the 1-D case. In the 2-D case, these results are computed at $(0.5, 1.0)$ on the north boundary. To compare the results of the 2-D code with that for 1-D case with collimated radiation, for results in Fig. 2c, the aspect ratio $\frac{X}{Y}=100$ was considered and the domain was divided into 500×10 control volumes. With diffuse radiation (Fig. 2d), the aspect ratio $\frac{X}{Y}=10$ was found sufficient. A higher value of $\frac{X}{Y}$ in case of collimated radiation is attributed to strong directional dependency.

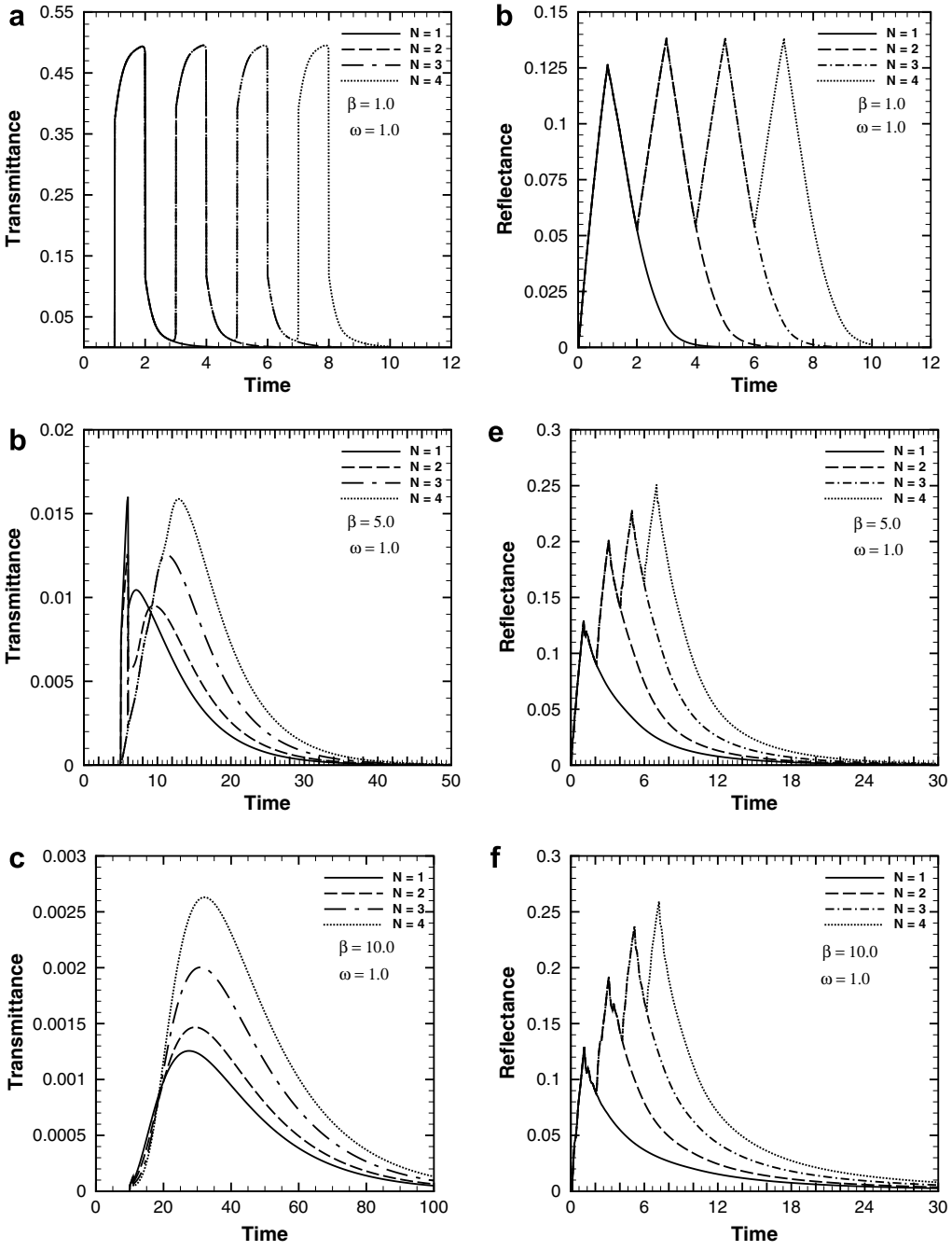

Fig. 4. Transmittance $q_t^*(0.5, 1.0, t^*)$ signals and reflectance $q_r^*(0.5, 0.0, t^*)$ signals for 1–4 pulses for three different values of extinction coefficient β. The south boundary subjected to collimated radiation.

It is seen from Figs. 2a–d that in all the case, results of the present work with single-pulse are in good agreement with those available in the literature.

3.2. Results with 1–4 pulse train

In the following pages, we provide results for a square medium ($\frac{X}{Y}=1$) with its south boundary subjected to either diffuse or collimated pulses. The pulse train is considered consisting of 1–4 pulses.

With the south boundary subjected to a diffuse pulse, Figs. 3a–f show transmittance $q_t^*(0.5,1.0,t^*)$ and reflectance $q_r^*(0.5,1.0,t^*)$ at the middle of the south and the north boundaries, respectively. With scattering albedo $\omega=1.0$, for 1–4 pulses, these results are shown for three values of the extinction coefficient β. It is seen from Figs. 3a–c that the magnitudes of the signals peak decrease with increase in β. It is also observed that troughs that are present in 2-4 pulses in Fig. 3a for $\beta=1.0$, vanish for higher values of β (Figs. 3b and c). Observations of Figs. 3a–c show that the peaks of different pulse-trains are more aligned for higher β and temporal spreads in the signals are more spread for higher β. A distinct difference in the peak magnitudes of the signals for multiple pulses are

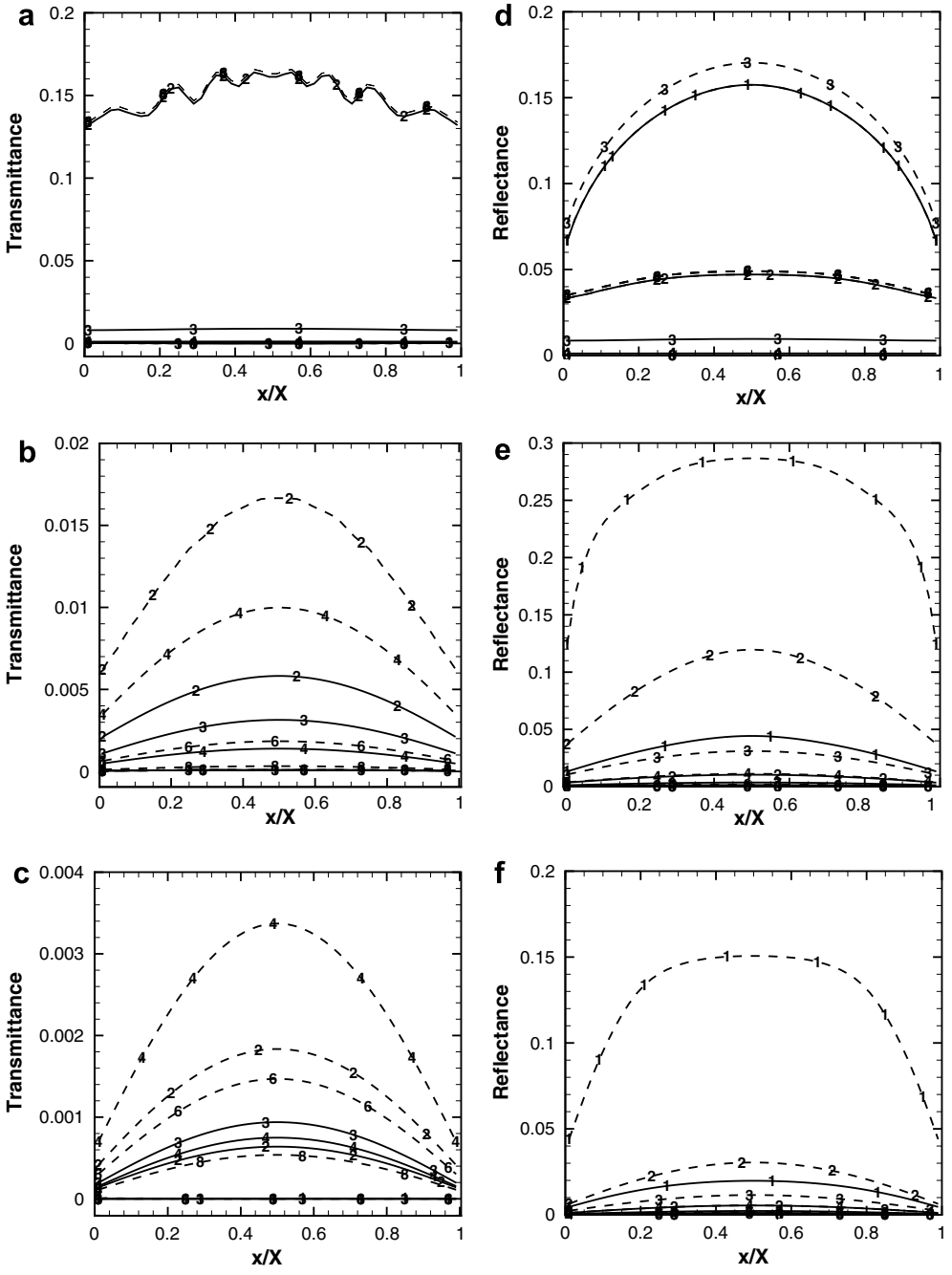

Fig. 5. Time evolution of the distribution of transmittance $q_t^*(x/X,1.0,t^*)$ and reflectance $q_r^*(x/X,0.0,t^*)$ signals along the boundaries. The digit n on any curve indicates the distribution of the signal at $n\times 100$th time step. Solid and dash lines are results for 1- and 4-pulse diffuse radiation.

observed for $\beta = 5.0$ and 10.0. Further, since radiation takes $t^* = \beta ct = \beta Y$ to reach the opposite (north boundary), with $Y = 1.0$, in Figs. 3a–c, the transmittance signals start appearing at $t^* = \beta$.

For the corresponding cases, reflectance $q_r^*(0.5, 0.0, t^*)$ results are shown in Figs. 3d–f. Unlike transmittance$q_t^*(0.5, 1.0, t^*)$, the peak magnitudes of the reflectance $q_r^*(0.5, 0.0, t^*)$ signals increase with increase in β, and also different crests and troughs are distinct for all values ofβ. Like transmittance $q_t^*(0.5, 1.0, t^*)$ (Fig. 3a), the reflectance $q_r^*(0.5, 0.0, t^*)$ signals (Fig. 3d) do not last long for $\beta = 1.0$, and for $\beta = 5.0$ and 10.0, they last longer (Figs. 3e and f). However, their temporal spans are shorter than the transmittance $q_t^*(0.5, 1.0, t^*)$ signals (Figs. 3b and c). Since the south boundary starts getting radiation the time the radiation enters the medium, the reflectance signals are seen to start with $t^* = 0.0$ (Figs. 3d–f).

Transmittance $q_t^*(0.5, 1.0, t^*)$ and reflectance $q_r^*(0.5, 0.0, t^*)$ results with collimated pulses are shown in Figs. 4a–f. With scattering albedo $\omega = 1.0$, for 1–4 pulses, these results are shown for three values of the extinction coefficient $\beta = 1.0$, 5.0 and 10.0. For $\beta = 1.0$, trends of

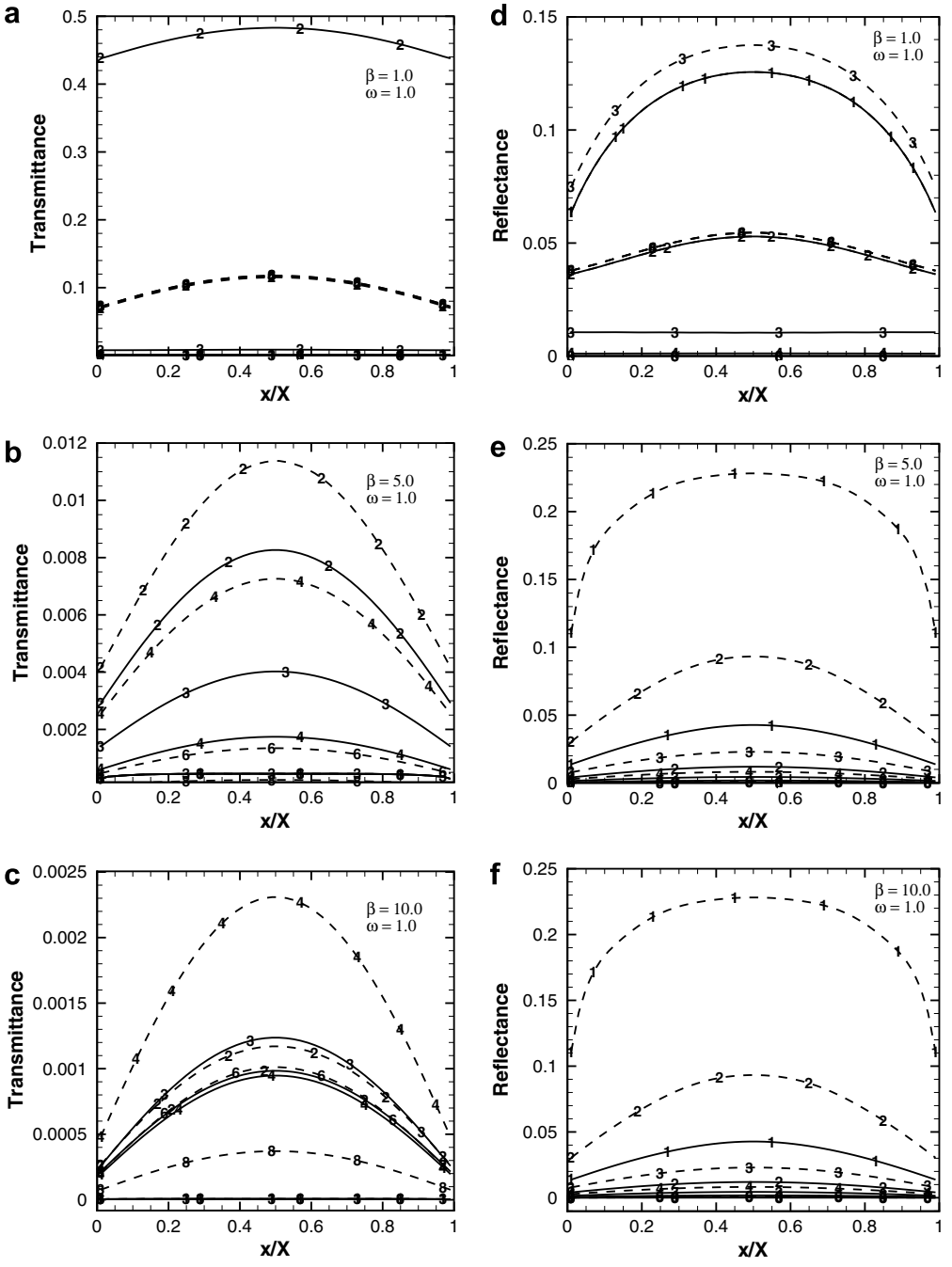

Fig. 6. Time evolution of the distribution of transmittance $q_t^*(x/X, 1.0, t^*)$ and reflectance $q_r^*(x/X, 0.0, t^*)$ signals along the boundaries. The digit n on any curve indicates the distribution of the signal at $n \times 100$th time step. Solid and dash lines are results for 1- and 4-pulse collimated radiation.

the two signals (Figs. 4a and d) are similar to that of diffuse pulse train (Figs. 3a and d). For 1–3 pulses, the transmittance signals with $\beta = 5.0$ have a distinct peak and a sharp decline leading to another well distributed maxima (Fig. 4b). The sharp peak is attributed to the arrival of the collimated component of the incident radiation much earlier than the diffuse radiations from the medium. Though the troughs in the curves occur at the same time for 1–4 pulses (Fig. 4b), a large difference in their magnitude is observed. With $\beta = 10.0$ (Fig. 4c), unlike $\beta = 5.0$ (Fig. 4b), distinct crests and troughs at an early stage are not prominent. Like diffuse radiation (Fig. 3c), for $\beta = 10.0$, the signals are characterized by a single crest for any number of pulses.

The reflectance $q_r^*(0.5, 0.0, t^*)$ results with $\beta = 1.0$, 5.0 and 10.0 for 1–4 pulses are shown in Figs. 4c–f, respec-

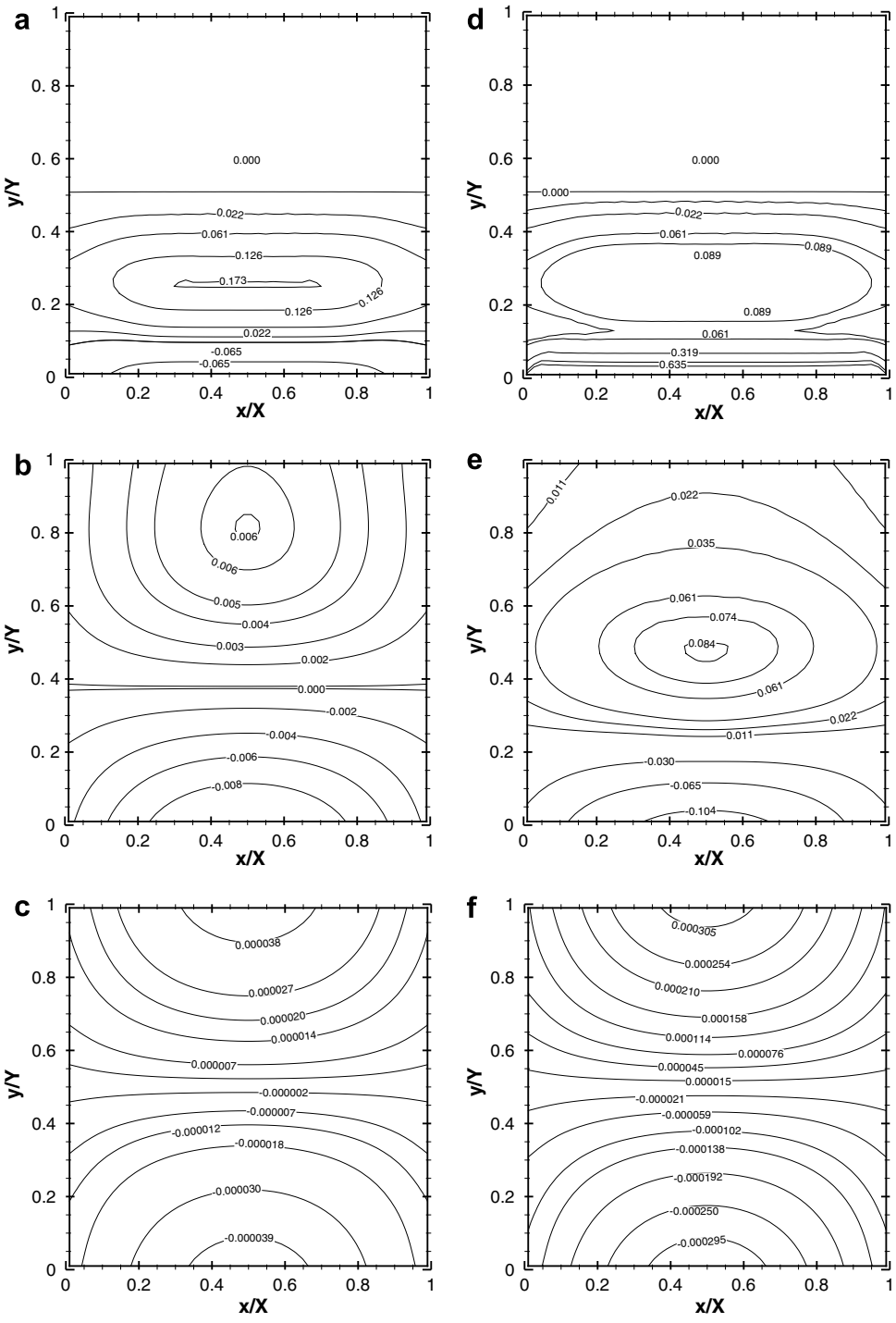

Fig. 7. Heat flux contours in the medium at time $\frac{t^*}{\Delta t^*}$ (a) = 50, (b) = 200, (c) 800 for a single-pulse, (d) = 50, (e) = 200, (f) 800 for a 4-pulse train. The south boundary subjected to diffuse radiation. $\beta = 1.0$, $\omega = 1.0$.

tively. Profiles of these signals are the same as that for the diffuse pulse train (Figs. 3d–f) except for $\beta = 5.0$ and 10.0, narrow crests and troughs are visible for a single and a 2-pulse train.

In Figs. 5 and 6, for a single and a 4-pulse train, distributions of transmittance $q_t^*\left(\frac{x}{X}, 1.0, t^*\right)$ and reflectance $q_r^*\left(\frac{x}{X}, 0.0, t^*\right)$ results along the boundaries, have been plotted for diffuse and collimated radiations, respectively. With $\omega = 1.0$, these distributions are shown for the extinction coefficient $\beta = 1.0$, 5.0 and 10.0. For a given β, these distributions are plotted at 6 time levels, viz. $\frac{t^*}{\Delta t^*} = 100, 200, 300, 400, 600$ and 800.

It is seen from Figs. 5a and 6a that when the medium is less participating ($\beta = 1.0$), the transmittance $q_t^*\left(\frac{x}{X}, 1.0, t^*\right)$ results for a single and a 4-pulse train almost coincide with each other at all times. However, the reflectance $q_r^*\left(\frac{x}{X}, 0.0, t^*\right)$ signals are more distinct at almost all times for a single and a 4-pulse train. For $\beta = 5.0$ and 10.0, the

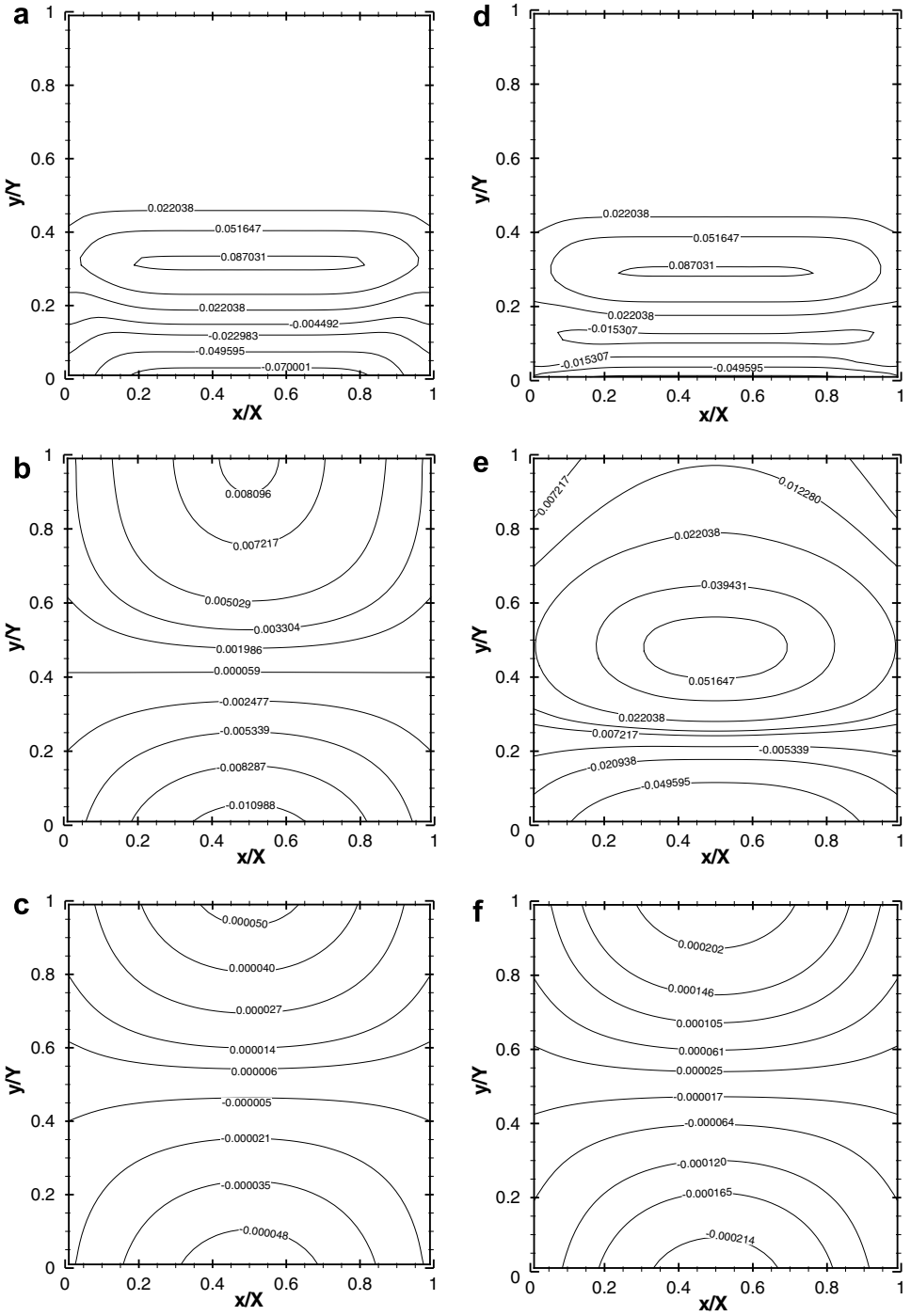

Fig. 8. Heat flux contours in the medium at time $\frac{t^*}{\Delta t^*}$ (a) = 50, (b) = 200, (c) 800 for a single-pulse, (d) = 50, (e) = 200, (f) 800 for a 4-pulse train. The south boundary subjected to collimated radiation. $\beta = 1.0$, $\omega = 1.0$.

transmittance $q_t^*\left(\frac{x}{X}, 1.0, t^*\right)$ signals at all time levels are well separated. However, it is observed that for any value of β, at an early stage $\frac{t^*}{\Delta t^*} = 100$ since the magnitudes of the signals are very small, they are not noticeable. This can be verified from Figs. 3a–c and 4a–c, where the time evolution of the transmittance signals in the middle of the north boundary (0.5, 1.0) have been plotted.

It is observed from Figs. 5d and 6d that for $\beta = 1.0$ at $\frac{t^*}{\Delta t^*} = 100$, for both diffuse and collimated pulses, profiles of the reflectance $q_r^*\left(\frac{x}{X}, 0.0, t^*\right)$ signals coincide for both a single and 4-pulse train. However, at $\frac{t^*}{\Delta t^*} = 300$, the $q_r^*\left(\frac{x}{X}, 0.0, t^*\right)$ is considerably higher for a 4-pulse train. At later times, they are close with each other. For $\beta = 5.0$ and 10.0, (Figs. 5e and f and 6e and f), profiles of

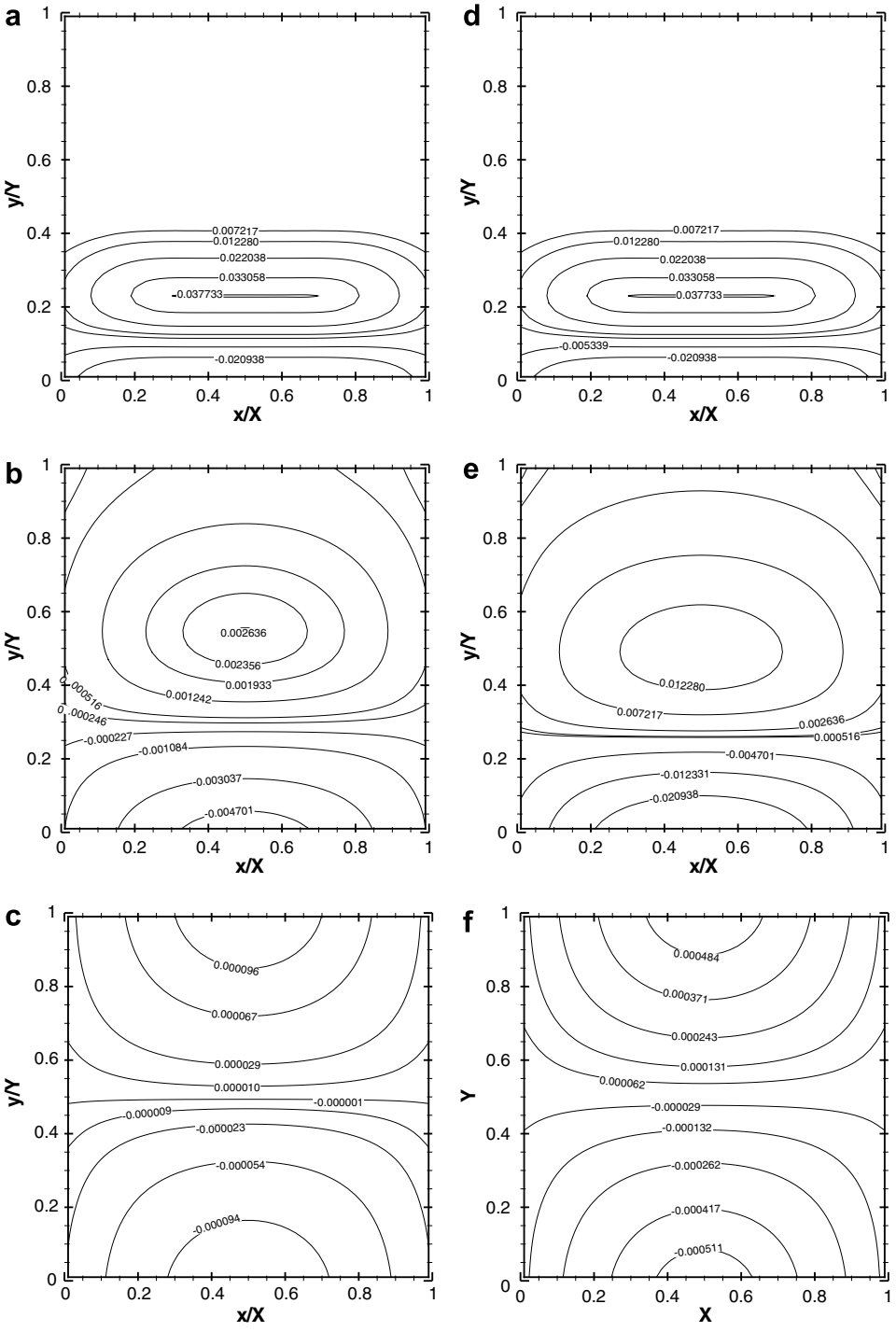

Fig. 9. Heat flux contours in the medium at time $\frac{t^*}{\Delta t^*}$ (a) = 50, (b) = 200, (c) 800 for a single-pulse, (d) = 50, (e) = 200, (f) 800 for a 4-pulse train. The south boundary subjected to diffuse radiation. $\beta = 10.0$, $\omega = 1.0$.

$q_r^*\left(\frac{x}{X}, 0.0, t^*\right)$ at the first two time levels are far too distinct for a 4-pulse train. However, for a single-pulse, their magnitudes are less. At later time levels, for both a single-pulse and a 4-pulse train, results are close to each other.

Figs. 7–10 provide heat flux contours in the medium for a single and a 4-pulse train. In each of these figures, the contours are plotted at three time levels, viz $\frac{t^*}{\Delta t^*} = 50, 200$ and 800. In these figures, results for a single-pulse are given in Figs. 7a–c, 8a–c, 9a–c and 10a–c, whereas the same for a 4-pulse train are given in Figs. 7d–f, 8d–f, 9d–f and 10d–f. For $\omega = 1.0$ and $\beta = 1.0$, heat flux contours are given in Figs. 7 and 8 for diffuse and collimated pulses, respectively. In Figs. 9 and 10, heat flux contours are presented for diffuse and collimated pulses, respectively for $\omega = 1.0$ and $\beta = 10.0$.

From Figs. 7a and 8a it is observed that for a single-pulse, at $\frac{t^*}{\Delta t^*} = 50$, the negative heat flux $q^*\left(\frac{x}{X}, \frac{y}{Y}, t^*\right)$ appears

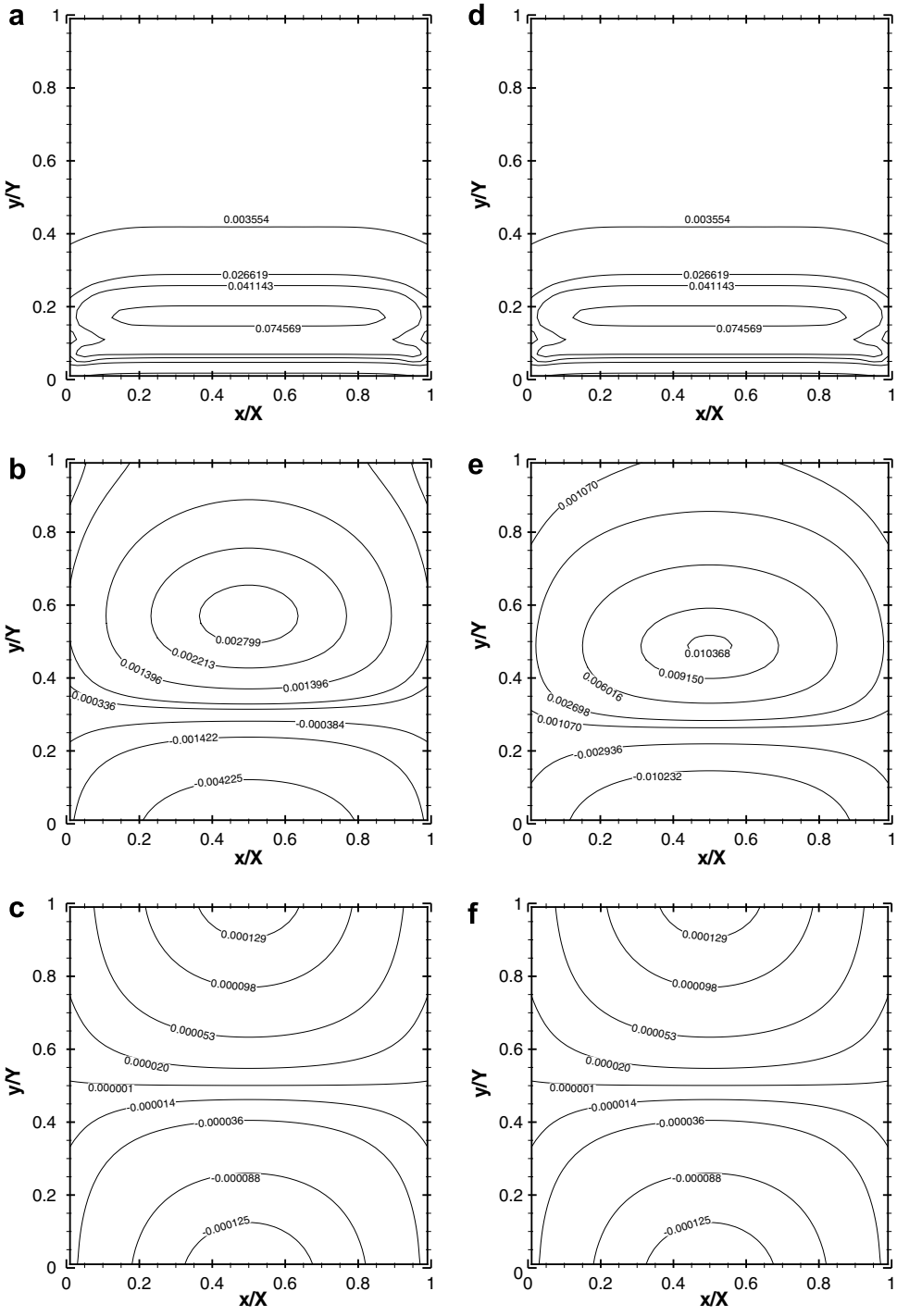

Fig. 10. Heat flux contours in the medium at time $\frac{t^*}{\Delta t^*}$ (a) = 50, (b) = 200, (c) 800 for a single-pulse, (d) = 50, (e) = 200, (f) 800 for a 4-pulse train. The south boundary subjected to collimated radiation. $\beta = 10.0$, $\omega = 1.0$.

near the south boundary. It is to be noted that the negative heat flux contributes towards the reflectance $q_r^*\left(\frac{x}{X}, 0.0, t^*\right)$ signals. For a 4-pulse train, from Fig. 7d it is observed that at $\frac{t^*}{\Delta t^*} = 50$, like Fig. 7a, for a single-pulse, the radiation has not reached the north boundary, but the positive heat flux towards the north boundary is more prominent.

At $\frac{t^*}{\Delta t^*} = 200$, it is observed from Figs. 7b and e and 8b and e that both negative and positive heat fluxes remain in the medium for a single and a 4-pulse train. The region of negative heat flux is observed to be more for a single-pulse. Further it is observed that the peak magnitudes of the heat flux are still found inside the medium in the neighborhood of the north boundary. But as time progresses $\left(\frac{t^*}{\Delta t^*} = 800\right)$, the maximum magnitude of heat flux is found to be concentrated around the middle of the south and the north boundaries as seen in Figs. 7c and f. This observation is substantiated with Figs. 5a and d.

A comparison of Figs. 7b and 8b show that the heat flux concentration around the middle of the north boundary is already established at $\frac{t^*}{\Delta t^*} = 200$ in the case of collimated single-pulse (Fig. 8b). Though the medium is low absorbing ($\beta = 1.0$), in case of collimated radiation, since radiation is

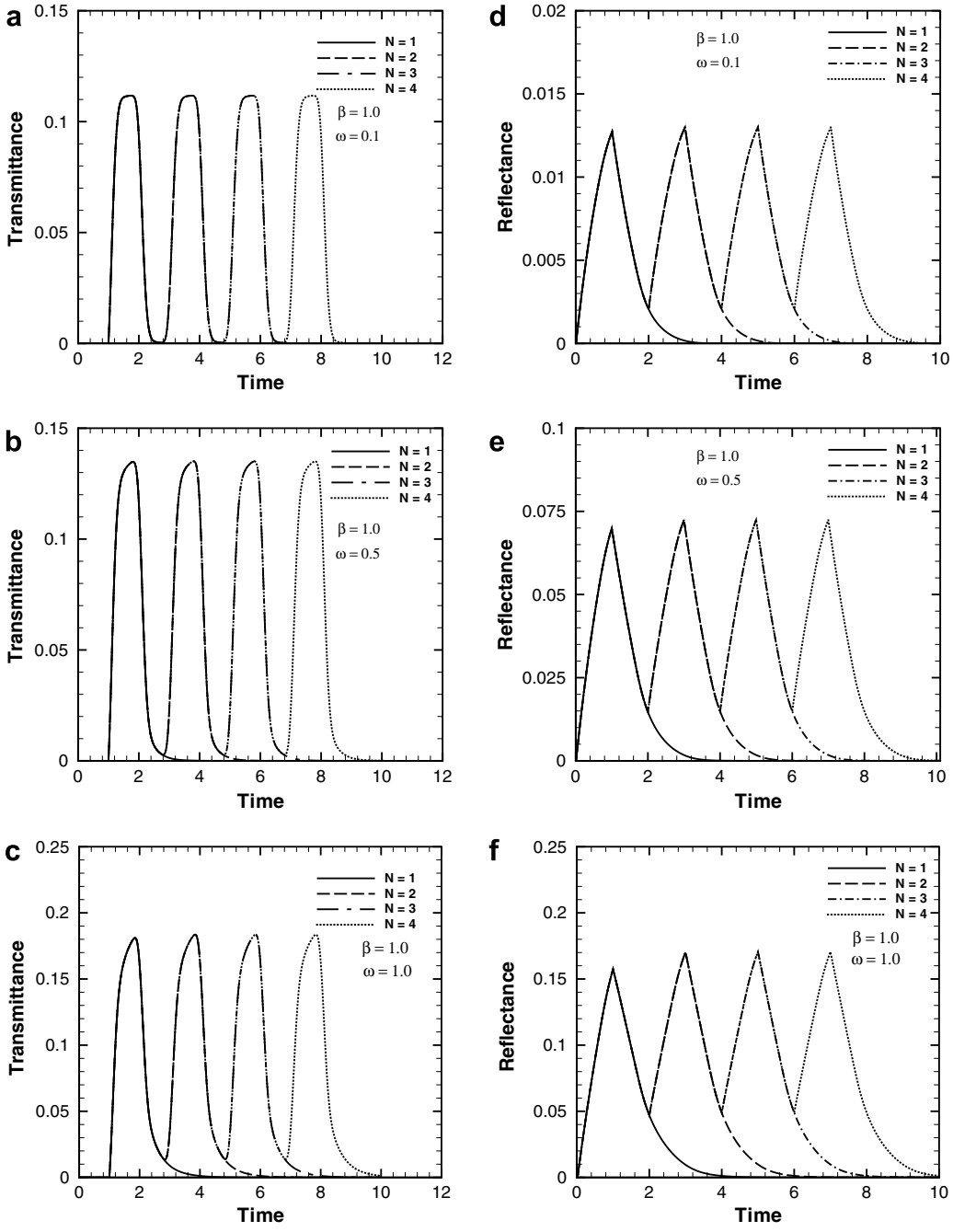

Fig. 11. Transmittance $q_t^*(0.5, 1.0, t^*)$ signals and reflectance $q_r^*(0.5, 0.0, t^*)$ signals for 1–4 pulses for three different values of scattering albedo ω. The south boundary subjected to diffuse radiation.

more directional than the diffuse, the heat packet is found much earlier at the north boundary (Fig. 8b).

Heat flux contours in Figs. 9a and d for diffuse radiation for a single-pulse and a 4-pulse train for $\beta = 10.0$ look similar at $\frac{t^*}{\Delta t^*} = 50$. A similar trend is also observed in Figs. 10a and d for the collimated radiation.

At $\frac{t^*}{\Delta t^*} = 200$, a smooth distribution of heat flux varying from a minimum near the boundaries to a maximum near the geometric centre of the medium is seen from Figs. 9b and e and 10b and e. The magnitude of the maximum is much higher in the case of Figs. 9e and 10e due to more energy contained with a 4-pulse train. The low gradient of heat flux inside the medium accounts for a longer life of both the signals with $\beta = 10.0$.

At $\frac{t^*}{\Delta t^*} = 800$, in Figs. 9c and 10c and f, the heat flux concentrations at the boundaries are widely distributed around the middle of the north and the south boundaries. The curves marked 8 in Figs. 5c and f and 6e and f are analogous to this observation.

With extinction coefficient $\beta = 1.0$, for 1–4 pulse trains, transmittance $q_t^*(0.5, 1.0, t^*)$ and reflectance $q_r^*(0.5, 0.0, t^*)$ signals for three different values of the scattering albedo ω are shown in Figs. 11 and 12 for diffuse and collimated radiations, respectively. It is seen from these figures (Figs.

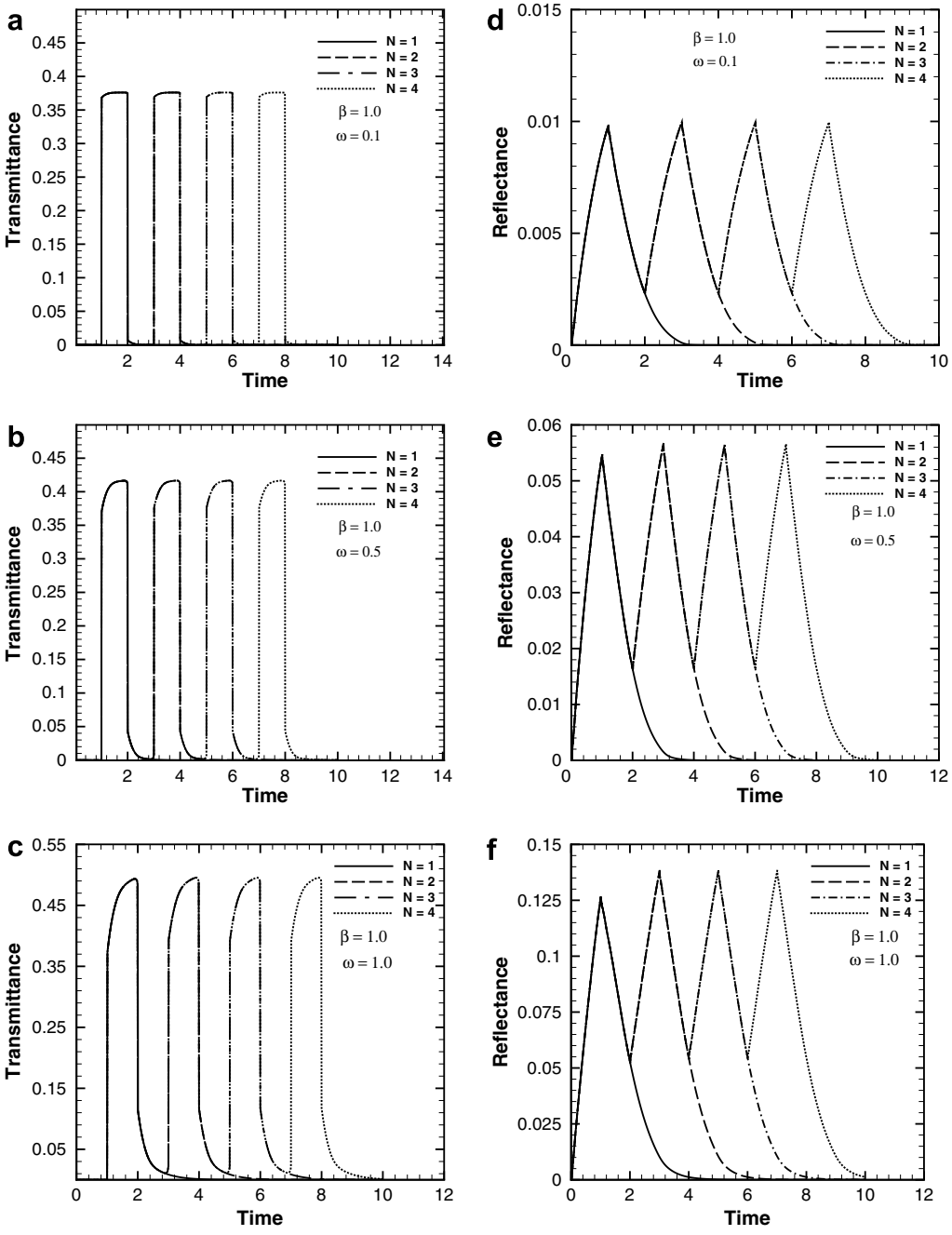

Fig. 12. Transmittance $q_t^*(0.5, 1.0, t^*)$ signals and reflectance $q_r^*(0.5, 0.0, t^*)$ signals for 1–4 pulses for three different values of scattering albedo ω. The south boundary subjected to collimated radiation.

11a–c and 12a–c) that when the scattering is less ($\omega = 0.1$), transmittance $q_t^*(0.5, 1.0, t^*)$ signals for a N-pulse train lasts for a shorter duration, their peaks are flattened and magnitudes of the peaks are less. A comparison of reflectance $q_r^*(0.5, 0.0, t^*)$ signals show, no visible effect of ω on the shape of the peaks and temporal spans for any pulse train. Like transmittance, the magnitudes of the reflectance signals too are found to increase with increase in ω. A comparison of Figs. 11 and 12 shows that in case of collimated radiation, the transmittance signals are the replicas of the incidence square pulse but with a considerable reduction in magnitude. Since the collimated radiation is more directional, the shape of the transmittance signals (Fig. 12a) for a lower value of β and a small value of ω is more or less like that of the incident pulses (Fig. 1d). However, in case of diffuse radiation, the incident energy is equally distributed in all directions, the signal profiles are of diffuse nature.

4. Conclusions

Transport of a train of short-pulse radiation through a 2-D rectangular participating medium was studied. The analysis was done by considering the south boundary of the medium subjected to a short-pulse radiation. With pulse width of the incident radiation of the order of a nano-second, the problem considered both diffuse and collimated radiations. The temporal profile of the pulse radiation was a step function and the pulse train consisted of 1–4 pulses. The homogeneous participating medium was absorbing and scattering. The finite volume method was used to analyze the problem. The transmittance and reflectance signals were studied for the effects of the extinction coefficient and the scattering albedo. Heat flux distributions inside the medium were also studied. With a single-pulse, results of the present work were compared with those available in the literature. The 1-D results from the 2-D code were also validated against 1-D results available in the literature. In all the cases, very good comparisons were obtained. Results with 1–4 pulses were found to have significant effects of the extinction coefficient and scattering albedo.

References

[1] C.L. Tien, A. Majumdar, F.M. Gerner, Microscale Energy Transfer, Taylor and Francis, Washington, DC, 1997.

[2] S. Kumar, K. Mitra, Microscale aspects of thermal radiation transport and laser applications, Adv. Heat Transfer 33 (1999) 187–294.

[3] L.S. Bass, M.R. Treat, Laser tissue welding: A comprehensive review of current and future applications, Lasers Surg. Med. 17 (1995) 315–349.

[4] K.H. Kim, Z. Guo, J.K.-J. Li, S. Kumar, Radiation heat transfer in tissue welding and soldering with ultrafast lasers, in: Proc. of the IEEE 29th Annual Northeast Bioengineering Conference, NJIT-Newark, New Jersey, March 22 and 23, 2003, pp. 185–186.

[5] K. Kim, Z. Guo, Ultrafast radiation heat transfer in laser tissue welding and soldering, Numer. Heat Transfer A 46 (2004) 23–40.

[6] F.H. Loesel, F.P. Fisher, H. Suhan, J.F. Bille, Non-thermal ablation of neutral tissue with femto-second laser pulses, Appl. Phys. B 66 (1998) 121–128.

[7] Y. Yamada, Light-Tissue Interaction and Optical Imaging in Bio-Medicine, vol. 6, Beggel House, New York, 1995, pp. 1–59.

[8] M. Sakami, K. Mitra, T. Vo-Dinh, Analysis of short-pulse laser photon transport through tissues for optical tomography, Opt. Lett. 27 (2002) 336–338.

[9] Z. Guo, S.K. Wan, D.A. August, J. Ying, S.M. Dunn, J.L. Semmlow, Optical imaging of breast tumor through temporal log-slope difference mappings, Comput. Biol. Med. 36 (2006) 209–223.

[10] S.K. Wan, Z. Guo, Correlative studies in optical reflectance measurements of cerebral blood oxygenation, J. Quant. Spectros. Radiat. Transfer 98 (2006) 189–201.

[11] F. Liu, K.M. Yoo, R.R. Alfano, Ultra-fast laser pulse transmission and imaging through biological tissues, Appl. Opt. 32 (1993) 554–558.

[12] V.V. Kancharla, S.C. Chen, Fabrication of biodegradable polymeric micro-devices using laser micromachining, Biomed. Microdevices 4 (2002) 105–109.

[13] R.E. Walker, J.W. Mclean, Lidar equation for turbid media with pulse stretching, Appl. Opt. 38 (1999) 2384–2397.

[14] K. Mitra, J.H. Churnside, Transient radiative transfer equation applied to oceanographic lidar, Appl. Opt. 38 (1999) 889–895.

[15] K.J. Grant, J.A. Piper, D.J. Ramsay, K.L. Williams, Pulse lasers in particle detection and sizing, Appl. Opt. 33 (1993) 416–417.

[16] S.K. Wan, Z. Guo, S. Kumar, J. Aber, B.A. Garetz, Noninvasive detection of inhomogeneities in turbid media with time-resolved log-slope analysis, J. Quant. Spectros. Radiat. Transfer 84 (2004) 493–500.

[17] K. Mitra, M.S. Lai, S. Kumar, Transient radiation transport in participating media within a rectangular enclosure, J. Thermophys. Heat Transfer 11 (1997) 409–414.

[18] K. Mitra, S. Kumar, Development and comparisons of models for light-pulse transport through scattering-absorbing media, Appl. Opt. 38 (1999) 188–196.

[19] Z.M. Tan, P.F. Hsu, An integral formulation of transient radiative transfer, J. Heat Transfer 123 (2001) 466–475.

[20] Z. Guo, S. Kumar, Discrete-ordinates solution of short-pulsed laser transport in two-dimensional turbid media, Appl. Opt. 40 (2001) 3156–3163.

[21] M. Sakami, K. Mitra, P.F. Hsu, Analysis of light-pulse transport through two-dimensional scattering and absorbing media, J. Quant. Spectros. Radiat. Transfer 73 (2002) 169–179.

[22] P. Rath, S.C. Mishra, P. Mahanta, U.K. Saha, K. Mitra, Discrete transfer method applied to transient radiative problems in participating medium, Numer. Heat Transfer A 44 (2003) 183–197.

[23] S.K.Wan, Z. Guo, S. Kumar, Rapid diagnosis of inhomogeneity in turbid media, in: Proc. of 2003 ASME Int. Mechanical Engineering Congress & Exposition, Paper No.: IMECE2003-41576, Washington, DC, Nov. 16–21, 2003, pp. 1–6.

[24] J.C. Chai, P.F. Hsu, Y.C. Lam, Three-dimensional transient radiative transfer modeling using the finite volume method, J. Quant. Spectros. Radiat. Transfer 86 (2004) 299–313.

[25] S.C. Mishra, P. Chug, P. Kumar, K. Mitra, Development and comparison of the DTM, the DOM and the FVM formulations for the short-pulse laser transport through a participating medium, Int. J. Heat Mass Transfer 49 (2006) 1820–1832.

[26] T. Okutucu, Y. Yener, Radiative transfer in participating media with collimated short-pulse Gaussian irradiation, J. Phys. D: Appl. Phys. 39 (2006) 1976–1983.

[27] T. Okutucu, Y. Yener, A.A. Busnaina, Transient radiative transfer in participating media with pulse-laser irradiation – an approximate Galerkin solution, J. Quant. Spectros. Radiat. Transfer 103 (2007) 118–130.

[28] Z. Guo, S. Kumar, Radiation element method for hyperbolic radiative transfer in plane – parallel inhomogeneous media, Numer. Heat Transfer B 39 (4) (2001) 371–387.

[29] C.Y. Wu, S.H. Wu, Integral equation formulation for transient radiative transfer in an anisotropically scattering medium, Int. J. Heat Mass Transfer 122 (2000) 818–822.
[30] Z.M. Tan, P.F. Hsu, Transient radiative transfer in three-dimensional homogeneous and non homogeneous participating media, J. Quant. Spectros. Radiat. Transfer 73 (2002) 181–194.
[31] X. Lu, P.F. Hsu, Reverse Monte Carlo simulations of light propagation in nonhomogeneous media, J. Quant. Spectros. Radiat. Transfer 93 (2005) 349–367.
[32] R. Muthukumaran, S.C. Mishra, Transient response of a planar participating medium subjected to a train of short-pulse radiation, Int. J. Heat Mass Transfer, accepted for publication.
[33] R. Muthukumaran, S.C. Mishra, Effect of a step short-pulse laser train on an inhomogeneous planar participating medium, Int. J. Heat Mass Transfer, submitted for publication.
[34] R. Muthukumaran, S.C. Mishra, Interaction of a short-pulse laser of a Gaussian temporal profile with an inhomogeneous medium, Numer. Heat Transfer Part A, accepted for publication.
[35] S.C. Mishra, H.K. Roy, Solving transient conduction–radiation problems using the lattice Boltzmann method and the finite volume method, J. Comput. Phys. 233 (2007) 89–107.
[36] J.C. Chai, S.V. Patankar, Finite volume method for radiation heat transfer, Adv. Numer. Heat Transfer 2 (2000) 110–135.